A fundamental test for MOND

Valerio Marra[1]⋆, Davi C. Rodrigues[1]† and Álefe O. F. de Almeida[1,2]‡

[1] *Núcleo de Astrofísica e Cosmologia, PPGCosmo & Dep. de Física, Universidade Federal do Espírito Santo, 29075-910, ES, Brazil*
[2] *IBM Brasil, 29055-131, Vitória, ES, Brazil.*

ABSTRACT
The Radial Acceleration Relation (RAR) shows a strong correlation between two accelerations associated to galaxy rotation curves. The relation between these accelerations is given by a nonlinear function which depends on an acceleration scale $a_†$. Some have interpreted this as an evidence for a gravity model, such as Modified Newtonian Dynamics (MOND), which posits a fundamental acceleration scale a_0 common to all the galaxies. However, it was later shown, using Bayesian inference, that this seems not to be the case: the a_0 credible intervals for individual galaxies were not found to be compatible among themselves. This type of test is a fundamental test for MOND as a theory for gravity, since it directly evaluates its basic assumption and this using the data that most favor MOND: galaxy rotation curves. Here we improve upon the previous analyses by introducing a more robust method to assess the compatibility between the credible intervals, in particular without Gaussian approximations. We directly estimate, using a Monte Carlo simulation, that the existence of a fundamental acceleration is incompatible with the data at more than 5σ. We also consider quality cuts in order to show that our results are robust against outliers. In conclusion, the new analysis further supports the claim that the acceleration scale found in the RAR is an emergent quantity.

Key words: Galaxy: kinematics and dynamic – galaxies: spiral – dark matter

1 INTRODUCTION

Several and diverse independent observations – spanning a large range of scales in space and time – strongly suggest the existence of some type of dark matter. The standard Cold Dark Matter (CDM) paradigm has been successful in providing relevant predictions and important insights. However, direct detection efforts are still inconclusive and many different dark matter candidates agree with the current observational and experimental bounds (e.g., Mo et al. 2010; Profumo 2017). Consequently, there is a large level of uncertainty as far as the status of the nature of dark matter is concerned.

The Radial Acceleration Relation (RAR) (McGaugh et al. 2016), which is closely related to the Mass Discrepancy-Acceleration Relation (Sanders 1990; McGaugh 2004; Milgrom 2016), shows a tight correlation between two accelerations associated to galaxy rotation curves: one is computed from the observed redshift and the other is the expected gravitational acceleration due to baryonic matter alone. The relation between these accelerations is given by

a nonlinear function that depends on an acceleration scale, labeled $a_†$. Milgrom (2016) and Li et al. (2018) have interpreted the appearance of this scale as evidence against CDM and in favor of the Modified Newtonian Dynamics (MOND) model that depends on a fundamental acceleration scale a_0, which numerically would be close to the value of $a_†$. On the other hand, different results within CDM are also capable of explaining, at least in part, the emergence of RAR (Ludlow et al. 2017; Navarro et al. 2017; Fattahi et al. 2018; Dutton et al. 2019). In particular, the tightness of the RAR, i.e. its dispersion, does not seem to be at odds with the CDM paradigm (Stone & Courteau 2019).

Rodrigues et al. (2018a, hereafter R18) have shown[1] that the RAR, rather than suggesting a fundamental a_0, actually provides strong evidence against the existence of such fundamental constant, implying that the $a_†$ scale must be emergent (among other examples of an emergent scale in the galaxy context, we recall the disk scale length). R18 was the first work that, in order to conclude on the universality of

---

⋆ E-mail: marra@cosmo-ufes.org
† E-mail: davi.rodrigues@cosmo-ufes.org
‡ E-mail: alefe@ibm.com

[1] See also McGaugh et al. (2018); Kroupa et al. (2018); Rodrigues et al. (2018b); Cameron et al. (2020); Rodrigues et al. (2020). For a different approach and with the same data, see also Frandsen & Petersen (2018); Zhou et al. (2020).

the acceleration scale, studied the (Bayesian) posterior distributions on the acceleration scales inferred from individual galaxies from a large dataset. For previous studies with error bars, usually defined from a given change on the χ^2 value with respect to its minimum, see Randriamampandry & Carignan (2014) and references therein. The result by R18 was subsequently confirmed by Chang & Zhou (2019), which repeated the R18 analysis considering the priors of Li et al. (2018). They directly confirmed that the latter priors also reject the fundamental acceleration hypothesis with high confidence (clearly beyond the 5σ level), these results are also in agreement with R18 and Rodrigues et al. (2018b). More recently, Zhou et al. (2020) have also provided further support.

Here, we improve upon the analysis of R18. First, we use the same priors and nuisance parameters that were used to support the existence of a fundamental a_0 in McGaugh et al. (2016) and Li et al. (2018). This set of priors is a physically reasonable choice, it was used in different works and it was shown to generate a_0 credible intervals for individual galaxies that are larger (and so more conservative) than those obtained with the set of priors adopted in R18 (see Rodrigues et al. 2018b, for further details). Second, and this is the main novelty of the present work, we go beyond the approximations that R18 adopted in order to quantify the tension between the posteriors on a_0 of the SPARC galaxies. We achieve the latter via an extension of the Verde et al. (2013) proposal. Our new results are not based on Gaussian approximations in order to compare the posteriors. With the new and more accurate method, we confirm here the findings of R18 that a fundamental acceleration scale is incompatible with rotation curve data. We add that the method here proposed is not specific to galaxy data and should be useful in other contexts as well.

This paper is organized as follows. In Section 2 we review the theory behind the fundamental acceleration scale a_0, while in Section 3 we discuss the observational data. In Section 4 we describe how we obtain and compare the posterior distributions on a_0, in Section 5 we summarize our numerical methods and our results are presented in Section 6. Section 7 is devoted to our conclusions. Technical details are given in Appendixes A, B and C.

2 THE RAR AND MOND

2.1 RAR for individual galaxies

Since the RAR is a tight correlation for rotationally supported galaxies (McGaugh et al. 2016) (tight in the sense that it spans about four orders of magnitude on the baryonic acceleration with a rms dispersion of about 0.1 dex), it is relevant to ask whether the $a_\dagger$ scale inferred from the RAR could be a universal scale for individual galaxies. In principle, this could unveil unexpected baryonic or dark matter properties. As shown by Li et al. (2018), for this same sample of galaxies, assuming that the RAR is relevant for individual galaxies with a common a_0 value given by $a_\dagger$, it is possible to infer a tighter correlation between the baryonic and observed accelerations. The latter is achieved if one considers best fits for the observed acceleration data and considering mass-to-light ratios, distance and inclination as nuisance parameters whose priors are compatible with the observational

errors stated by Lelli et al. (2016). From the assumption that the RAR is valid for individual galaxies, the latter analysis is capable of finding a residual scatter in the data which must be attributed to observational error, according the the starting hypothesis. However, this approach is not capable of concluding if the data is compatible with the assumption that the RAR is valid for individual galaxies. There is no logical necessity that the resulting minimization procedure, in spite of minimizing the scatter, would lead to a picture closer to reality than the original RAR approach (the use of observational errors to decrease a scatter may be an artificial procedure). Indeed, similar criticism was brought forward by Dutton et al. (2019); Stone & Courteau (2019).

2.2 MOND

Closely related to the hypothesis of the RAR being valid for individual galaxies is the Modified Newtonian Dynamics (MOND) hypothesis (Milgrom 1983; Famaey & McGaugh 2012). MOND assumes no dark matter in galaxies and is based on a non-linear relation between the physical acceleration ($\boldsymbol{a}$) and the Newtonian one ($\boldsymbol{a}_\mathrm{N}$), written as

$$\boldsymbol{a} = \nu\left(\frac{a_\mathrm{N}}{a_0}\right)\boldsymbol{a}_\mathrm{N}\,, \tag{1}$$

where ν is a function, commonly called the (inverse) interpolating function of MOND, and a_0 would be a fundamental constant with dimension of acceleration. The interpolating function needs to be such that for large accelerations ($a_\mathrm{N} \gg a_0$) one finds standard Newtonian gravity (i.e., $a = a_\mathrm{N}$), while for small accelerations ($a_\mathrm{N} \ll a_0$) one finds the so-called deep-MOND regime. The deep-MOND regime is taken to be $a = \sqrt{a_0 a_\mathrm{N}}$, which implies that far from the object of mass M the circular velocity of a test particle is independent on its distance from M: $V^2 = \sqrt{a_0 G M}$, where G is the (Newtonian) gravitational constant. The latter behavior was originally motivated from the Tully-Fisher relation (Milgrom 1983), while more recently other related motivations were put forward (e.g., Milgrom 2015).

2.3 A fundamental test of MOND

In order to apply MOND to individual galaxies, the first step is to select a ν function and a value for the acceleration scale a_0. Different approaches can be found in the literature (Milgrom 1983; Famaey & McGaugh 2012), each one with its pros and cons. The most common approach is to choose a simple function that satisfies the asymptotic properties for being the interpolating function, and then perform rotation curve fits for several galaxies with a_0 taken as a free parameter. The global value of a_0 is then taken to be certain average (such as the median) over all the best-fit a_{0g} values (where the index g was added to indicate the value of a_0 for the g-th galaxy). Assuming that the galaxy sample is a representative one, the resulting global a_0 value depends on the adopted interpolating function ν and on how the uncertainties of the baryonic parameters were handled. In the end, with reasonable considerations, the result is $a_0 \sim 10^{-13}\,\mathrm{km/s}^2$. See, for instance, R18 (supplementary material) and Gentile et al. 2011.

For a given ν function, the determination of the global a_0 value from such procedure is not optimal: it neglects the

information from the individual a_{0g} uncertainties, i.e., the a_{0g} posterior distributions. Actually, not only one has the chance of finding the most accurate global a_0 value, from these posteriors one can also perform *the most fundamental test of MOND for a given interpolating function, namely: to analyze the compatibility of the existence of a fundamental acceleration scale with the observational data.*

Before concluding this subsection, we remark that the issue of constancy of a_0 among different galaxies is not a new one. In particular, Kent (1987) singled out a factor 5 discrepancy between the best-fit a_{0g} values from different galaxies, which lead Milgrom (1988) to point out possible physical issues as the cause of such discrepancy. Milgrom (1988) also claimed that using a_0 as a free parameter should be deprecated, apart from the purpose of determining the best overall a_0 value. Perhaps, at the time, this research field was not yet ready for such tests (e.g., due to Bayesian methods being uncommon and due to the lack of computational power), but currently we understand that there is no justification to avoid this fundamental test. We also point out that in R18 and here we find a discrepancy of about 2 orders of magnitude among the best-fit a_{0g} values from individual galaxies.

2.4 RAR-inspired interpolating function

The RAR itself provides a data-driven choice for the interpolating function. If MOND is true, the most sensible way of specifying an interpolating function at galaxy level seems to be looking for RAR-like data, which already displays a correlation between baryonic and observational acceleration with a minimum set of assumptions on the observational data. The most simple and precise analytical function currently known capable of describing the correlation is given by (McGaugh et al. 2016)

$$\boldsymbol{a} = \frac{\boldsymbol{a}_{\mathrm{N}}}{1 - e^{-\sqrt{a_{\mathrm{N}}/a_0}}}. \tag{2}$$

Here we adopt this interpolating function, which we call the RAR-inspired interpolating function, but with an *a priori* unknown value for a_0. We do not assume that the acceleration scale is the one found from the RAR ($a_\dagger$), thus in the above we use a_0. In R18 we considered two other interpolating functions commonly used in the MOND context, but our results are essentially the same for any of them (the RAR-inspired interpolating function (2) has a slightly smaller RAR dispersion and fares slightly better with respect to a common acceleration scale).

3 OBSERVATIONAL DATA MODELING

Here we use the SPARC data (Lelli et al. 2016) for rotationally supported galaxies, which were the same data used to derive the RAR (McGaugh et al. 2016). The same quality cuts applied to the original 175 SPARC galaxies are also applied here, namely that galaxies with inclinations smaller than $30°$ and those with relevant asymmetries are not considered (i.e., those with quality flag Q=3). This leads to a sample of 153 galaxies, which we call the RAR sample.

Since dark matter is not being considered, the Newtonian acceleration only has the baryonic component, which is subdivided into two main parts: stellar and atomic gas components (the latter composed by hydrogen and helium mainly; while the former is decomposed into a disk and a bulge components). The centripetal Newtonian acceleration, as inferred from the baryonic distribution, can be decomposed as

$$a_{\mathrm{N}} = \Upsilon_{\mathrm{b}} a_{\mathrm{b}} + \Upsilon_{\mathrm{d}} a_{\mathrm{d}} + a_{\mathrm{gas}}. \tag{3}$$

Where a_{b} and a_{d} refer to the bulge and disk contributions to the centripetal acceleration for mass-to-light ratios (Υ_{b} and Υ_{d}) equal to one. Equivalently, but closer to the provided SPARC data,

$$V_{\mathrm{N}}^2 = \Upsilon_{\mathrm{b}} |V_{\mathrm{b}}| V_{\mathrm{b}} + \Upsilon_{\mathrm{d}} |V_{\mathrm{d}}| V_{\mathrm{d}} + |V_{\mathrm{gas}}| V_{\mathrm{gas}}. \tag{4}$$

In the above, we use $V_x |V_x|$ in place of V_x^2 since it is customary (and the SPARC database uses this convention) to use negative values of V_x to represent negative contributions to the centripetal acceleration; thus, $V_x(R) < 0$ means that $a_x < 0$, implying that one should write $a_x = V_x |V_x|/R$. If, for a given R, $V_{\mathrm{N}}^2 < 0$, then there is no Newtonian rotation curve at that radius.

Since MOND effectively amplifies the acceleration inferred from the baryons, uncertainties on the baryonic data have larger impact than in dark matter models. The baryonic parameters whose uncertainties have larger dynamical effect on the inferred circular velocity from MOND are commonly taken to be the stellar mass-to-light ratios (Υ_{d}, Υ_{b}), galaxy distance (D) and lastly galaxy inclination (I) (e.g., Gentile et al. 2011; McGaugh et al. 2016). We remark that R18 considered I as fixed, since this additional parameter would not impact the conclusions in that paper. There is also an additional technical reason for R18 to be especially economic on the number of nuisance parameters: R18 explored the Bayesian posteriors on a grid, which is a very robust way of sampling the tails of the distributions ($> 3\sigma$ credible regions). However, the discretization of the parameter space is computationally demanding, and any new parameter would at least multiply the necessary computational time by a factor $\mathcal{O}(100)$. Hence, for a larger number of parameters, MCMC methods become necessary and we apply them here (with a lot of care on convergence issues).

The dynamical impact of changes on Υ is already explicit in eq. (4), which should be combined with eq. (2). A distance change from D_0 to D due to a factor δ_D (i.e., $D = \delta_D D_0$) implies that: *i)* the galaxy coordinate radius is stretched by δ_D ($R' = \delta_D R$); *ii)* the luminosity and hence the mass are increased such that the Newtonian acceleration is invariant, and *iii)* there are no changes on the galaxy spectra, hence on the observational circular velocity. In summary (see e.g., supplementary material of R18 and Li et al. 2018 for further details),

$$V_{\mathrm{N}}'(R') = \sqrt{\delta_D} V_{\mathrm{N}}(R) \text{ and } V_{\mathrm{C}}'(R') = V_{\mathrm{C}}(R). \tag{5}$$

Distance changes do not change the circular velocity V_{C} (in the sense above), or its errors. It is common to designate V_{C} as the observed velocity ("V_{Obs}"). However, since we are here considering inclination changes, which change the value of the latter, V_{C} seems to be a good choice.

The circular velocity depends on the redshift data and on the galaxy inclination (since the redshift only gives line-of-sight velocity information). An inclination change from I_0 to I changes V_{C} and the corresponding error σ_V, which are

given by (e.g., de Blok & McGaugh 1998; Lelli et al. 2016; Li et al. 2018)

$$V_{\rm C}' = V_{\rm C}\frac{\sin I_0}{\sin I} \quad \text{and} \quad \sigma_V' = \sigma_V\frac{\sin I_0}{\sin I}\,. \tag{6}$$

4   STATISTICAL ANALYSIS

We will carry out Bayesian inference for the galaxies of the RAR sample (Lelli et al. 2016; McGaugh et al. 2016). The posterior distribution for a given galaxy data $f(\theta|\text{galaxy})$ with respect to the parameter vector θ is obtained via Bayes' theorem:

$$f(\theta|\text{galaxy}) = \frac{f(\theta)\,\mathcal{L}(\theta)}{\mathcal{E}}\,, \tag{7}$$
$$\theta = (A_0, Y_{\rm b}, Y_{\rm d}, D, I)\,,$$

where $f(\theta)$ is the prior, $\mathcal{L}(\theta)$ is the likelihood and $\mathcal{E}$ is the evidence. A brief review on Bayesian inference in this context can be found in the supplementary material of R18. We adopt the following set of independent variables for our analysis:

$$A_0 \equiv \log_{10}\left(\frac{a_0}{\text{km/s}^2}\right)\,, \tag{8}$$

$$Y_{\rm b} \equiv \log_{10}\Upsilon_{\rm b}\,, \tag{9}$$

$$Y_{\rm d} \equiv \log_{10}\Upsilon_{\rm d}\,, \tag{10}$$

besides galaxy distance D and inclination I.

The analysis of this paper focuses on the 1D marginalized posteriors on A_0 for each galaxy, which are obtained according to

$$f(A_0|\text{galaxy}) = \int f(\theta|\text{galaxy})\,{\rm d}Y_{\rm b}\,{\rm d}Y_{\rm d}\,{\rm d}D\,{\rm d}I\,. \tag{11}$$

4.1   Likelihood

For each galaxy, we adopt the Gaussian likelihood

$$\mathcal{L}(\theta) = |2\pi\Sigma|^{-1/2}e^{-\chi^2(\theta)/2}\,, \tag{12}$$

where Σ is the covariance matrix, to be detailed below, and $\chi^2 = \chi^2(A_0, Y_{\rm b}, Y_{\rm d}, D, I)$, with

$$\chi^2 = \sum_{i=1}^{N}\left(\frac{V_{\rm M}(R_i, A_0, Y_{\rm b}, Y_{\rm d}, D) - V_{{\rm C},i}\frac{\sin I_0}{\sin I}}{\sigma_{V,i}\frac{\sin I_0}{\sin I}}\right)^2\,. \tag{13}$$

In the above, N is the number of data points of the given galaxy data, $V_{\rm M}$ is the model circular velocity, R_i is the galaxy radius at which the reference circular velocity $V_{{\rm C},i}$ was measured. The corresponding error is $\sigma_{V,i}$. The quantities $V_{{\rm C},i}$ and $\sigma_{V,i}$ are provided by SPARC with the reference inclination I_0. The determinant of the (diagonal) covariance matrix is $|\Sigma| = \prod_i \sigma_{V,i}^2$.

The model velocity $V_{\rm M}$ is the one inferred from MOND using the interpolating function (2) and the Newtonian velocity (4) with the distance correction (5).

4.2   Priors

As commented in the Introduction, in this work we adopt, for the mass-to-light ratios, distance and galaxy inclinations,

essentially the same priors used by Li et al. (2018) and Chang & Zhou (2019).

Regarding the prior on A_0, we adopt a uninformative prior, a flat prior in this case, as MOND does not predict neither a value nor a distribution for A_0: it has to be inferred from observational data. In order to facilitate the comparison between our results and the results of other works, we recall that Li et al. (2018) considered two different priors for A_0, a flat one (just like we are considering here) and a very sharp Gaussian prior centered on the RAR $a_\dagger$ value (which, as expected, strongly restricted any variation on a_0 between galaxies). Chang & Zhou (2019) considered a Gaussian prior on A_0, but they considered it with a much larger dispersion (two orders of magnitude). Their Gaussian width is sufficiently large to include, at 1σ level, all (or almost all) the A_0 posterior modes found in R18 with a flat prior, hence that Gaussian prior is roughly equivalent to a flat prior.

Decomposing the prior $f(\theta)$ as follows

$$f(\theta) = f(A_0)f(Y_{\rm b})f(Y_{\rm d})f(D)f(I)\,, \tag{14}$$

the priors for each parameter read:

$$f(A_0) = 1/15\,, \qquad \text{with } -20 \leq A_0 \leq -5\,, \tag{15}$$

$$f(Y_{\rm b}) = \mathcal{N}(0.5, 0.1^2)\,, \tag{16}$$

$$f(Y_{\rm d}) = \mathcal{N}(0.7, 0.1^2)\,, \tag{17}$$

$$f(D) = \mathcal{N}(D_0, \sigma_D^2)\,, \qquad \text{with } D \geq 0.5 \text{ Mpc}\,, \tag{18}$$

$$f(I) = \mathcal{N}(I_0, \sigma_I^2)\,, \qquad \text{with } 1° \leq I \leq 90°\,. \tag{19}$$

The errors σ_D and σ_I vary from galaxy to galaxy according to the values provided by the SPARC dataset. The priors (15, 18, 19) have zero value outside the given ranges. The symbol $\mathcal{N}(x, \sigma_x^2)$ stands for a normal (Gaussian) distribution centered at x and with σ_x as the standard deviation (Gaussian root-mean-squared width). In the following, we detail further the priors above:

i) $f(A_0)$. We use a uniform prior with support in a large range. None of the galaxies have 5σ posterior distributions with $A_0 > -5$, while some galaxies have $A_0 < -20$, but such small values are dynamically equivalent to $a_0 = 0$ (or, $A_0 \to -\infty$); hence extending towards lower and finite values of A_0 would be inconsequential. For comparison, the global best value for A_0 is about -13, while -20 is indistinguishable from Newtonian gravity.

ii) $f(Y_{\rm b})$ **and** $f(Y_{\rm d})$. For the mass-to-light ratios (which are in the 3.6 μm band), we use the same central values and dispersions of McGaugh et al. (2016) and Li et al. (2018) (see also Meidt et al. (2014) and Querejeta & et al (2015)). These priors imply that $\Upsilon_{\rm b} > 0$ and $\Upsilon_{\rm d} > 0$, see eqs. (9-10).

iii) $f(D)$. It is the same prior used by Li et al. (2018), but with a constraint. The purpose of the latter is to restrict unrealistic degeneracies with the distance. The closest RAR galaxy has a distance of 0.98 ± 0.05 Mpc, but some galaxies at $\sim$40 Mpc have 1σ uncertainties of $\sim \pm 10$ Mpc. The distances of such galaxies were estimated from the Hubble flow, and this is why they have large relative distance errors. Eq. (18) states that none of the RAR galaxies is allowed to be closer than 0.5 Mpc (this is very conservative, Andromeda for instance is at 0.8 Mpc).

iv) $f(I)$. Since the observed inclination is defined in the range from $0°$ to $90°$, being $0°$ a face-on galaxy, we use the same constraints, but starting from $1°$. We recall that

$0°$ corresponds to a singularity (face-on galaxies have no rotation curve), and also that the RAR sample only includes galaxies with $I_0 \geq 30°$.

The constraints in the priors $f(D)$ and $f(I)$ have no impact on the best-fits, but they can reduce, for a few galaxies, the tails of the A_0 posteriors. These constraints are irrelevant for most of the galaxies, they are small deviations from pure Gaussian distributions, and, for few cases, they imply minor improvements from the physical perspective, due to the removal of unrealistic cases. The numerical analysis benefits from these constraints, since they impose a small but finite parameter distance from the singularities $D = 0$ and $i = 0°$.

4.3 Quality cuts

All the galaxies that we consider are from the SPARC sample (175 galaxies). More specifically, we only use those galaxies used to determine the RAR (153 galaxies). Reducing the sample from the SPARC to the RAR sample is the first quality cut that we use (Q_1): it eliminates galaxies whose reference inclination value is smaller than $30°$ (i.e., $I_0 < 30°$) and those galaxies with poor concordance between approaching and receding rotation curves, classified as $\mathcal{Q} = 3$ by Lelli et al. (2016). This is also the same quality cut adopted by Li et al. (2018). All the data that we provide here is subjected to this quality cut.

The Q_1 quality cut uses criteria based on physical data to eliminate galaxies that have a higher chance of providing less accurate A_0 determination. We also consider a second quality cut Q_2, whose main purpose is the same of Q_1, but whose criteria are based on statistical data that suggest that A_0 may have not been accurately determined for that galaxy. Q_2 is divided in the following two parts ($Q_2 = Q_{2a} \wedge Q_{2b}$):

- Q_{2a}, the compatibility of the model best fit with the observational data;
- Q_{2b}, the existence of well-defined 5σ credible regions in the range stated in eq. (15).

Regarding Q_{2a}, galaxies with high $\chi^2_{\min}$, whose p-value, considering a χ^2-statistics, is outside the expected 5σ region, are eliminated:

$$1 - p\text{-value} \equiv F_k(\chi^2_{\min}) \geq \text{erf}\, \frac{n = 5}{\sqrt{2}}, \quad (20)$$

where $F_k(\chi^2)$ is the cumulative χ^2-distribution with k degrees of freedom, $\chi^2_{\min}$ is the observed value and erf is the error function. In this case it is $k = N - M$ where N is the number of data points and M the number of fitted parameters, which is 4 or 5 depending on the presence of the bulge.[2] The reference p-value above is 5.7×10^{-7}. We stress that we only eliminate those with especially high $\chi^2_{\min}$ values; we do not assume that $\chi^2_{\min}$ values provide a good standard for

model comparison or quality of fits in general (Andrae et al. 2010); the assumption is that a too high χ^2 value is a qualitative sign that possibly something is wrong; if the model is assumed right, then the data is possibly problematic, therefore eliminating it may be safer.

For Q_{2b}, there are some galaxies for which $a_0 = 0$ is compatible with the data at 5σ level, leading to credible regions on A_0 that are not bounded from below. These galaxies would not improve the chances of a fundamental a_0 value, being "outliers" as far as MOND is concerned. Q_{2a} and Q_{2b} are evaluated for each galaxy and the results are shown in Table 1.

Although we always use Q_1, we evaluate our results both with and without Q_2. Therefore, Q_2 provides additional support that our results are robust against outliers, while being clear that our results do not depend on Q_2.

At last, we also stress that these quality cuts are applied homogeneously to all the sample. That is, we never re-analyze *a posteriori* the observational data, looking for case by case justifications for why particular galaxies did not provide some expected result. Any sample may always be subjected to some unknown relevant systematics, but our hope is that the observational data is being properly handled, with at most a few ill-modeled cases that would not contaminate the complete statistics. The Q_2 quality cut helps on providing an additional safety measurement against unknown systematics, and its application here implies a decrease on the sample size from 153 galaxies (the RAR sample) to 91 galaxies. This quality cut was introduced, in this galaxy context, in R18.

The sample composed by the SPARC galaxies with the Q_1 quality cut is labeled $\mathcal{S}_1$ (the RAR sample), while the sample with the two quality cuts, $Q_1 \wedge Q_2$, is labeled $\mathcal{S}_2$.

4.4 Global best value

After applying some set of quality cuts, one is left with N_G galaxies, indexed by g, from a subset $\mathcal{S}$ of the SPARC sample. Assuming a common A_0 value, we combine all the galaxy as follows:

$$f(A_0, \theta_1, ..., \theta_{N_\text{G}} | \mathcal{S}) = \frac{f(A_0, \{A_{0g}\}) \prod_{g=1}^{N_\text{G}} f(\theta_g) \mathcal{L}(\theta_g)}{\mathcal{E}}, \quad (21)$$

$$f(A_0, \{A_{0g}\}) = \delta(A_0 - A_{01}) \ldots \delta(A_0 - A_{0N_\text{G}}), \quad (22)$$

$$\theta_g = (A_{0g}, Y_{bg}, Y_{dg}, D_g, I_g).$$

where we used the fact that the galaxies' rotation curves are independent from each other. The vector θ_g is the analogue of θ, but indexed for each one of the galaxies. Priors and likelihoods are as in Eq. (7).

The prior of Eq. (22) imposes that all the A_{0g} are equal to A_0, and thus among themselves. One can then marginalize over the N_G variables A_{0g} so that one obtains a posterior that depends on A_0. Indeed, introducing

$$\hat{\theta}_g = (Y_{bg}, Y_{dg}, D_g, I_g), \quad (23)$$

we write,

$$f(A_0, \hat{\theta}_1 ... \hat{\theta}_{N_\text{G}} | \mathcal{S}) = \int \mathrm{d}A_{01} ... \mathrm{d}A_{0N_\text{G}}\, f(A_0, \theta_1, ..., \theta_{N_\text{G}} | \mathcal{S})$$

$$= \frac{f(A_0)^{N_\text{G}}}{\mathcal{E}} \prod_g f(\hat{\theta}_g) \mathcal{L}(A_0, \hat{\theta}_g). \quad (24)$$

---

[2] There are 4 galaxies (D512-2, NGC6789, UGC00634, UGC07232) that have $N = M = 4$ so that $F_k(\chi^2)$ is singular. If the model was linear, these galaxies would have $\chi^2_{\min} = 0$. As it is well known (Andrae et al. 2010), this does not happen as there are nonlinearities. In order to account for this we consider the effective number of parameters $M_\text{eff} = M - 1$. The consequence of using M_eff is that these 4 galaxies pass Q_{2a}.

Finally, it follows that the marginalized posterior on A_0 is proportional to the product of the marginalized posteriors on A_0 from the individual galaxies:

$$f(A_0|\mathcal{S}) = \frac{f(A_0)^{N_G}}{\mathcal{E}} \prod_g \int d\hat{\theta}_g f(\hat{\theta}_g) \mathcal{L}(A_0, \hat{\theta}_g)$$

$$= \frac{\prod_g \mathcal{E}_g}{\mathcal{E}} \prod_g f(A_0|\text{galaxy}_g) \equiv \frac{C}{\mathcal{E}} \prod_g f(A_0|\text{galaxy}_g), \quad (25)$$

where the evidences $\mathcal{E}_g$ are defined in eq. (7), and we defined the constant C. We call "global best value", and denote it by A_0^{gbv}, the value of A_0 that maximizes $f(A_0|\mathcal{S})$. That is, it is the mode of the A_0 distribution marginalized over all the other parameters.[3] A comment supporting this way of finding the best a_0 can also be found in Milgrom (1988). Note that this method (see the prior (22)) assumes rather than tests the existence of a universal parameter. In the following, we will instead assess the compatibility between the various galaxy posteriors on A_0.

In R18 we computed the global best value by approximating the posteriors $f(A_0|\text{galaxy}_g)$ as Gaussians and performing a χ^2 minimization. In practice, for this application, the difference is very small (see Table 2). However, we stress that the method here used is to be preferred to that of R18, since it does not rely on a Gaussian approximation for the mean and variance. Here we use the full posterior distribution up to 5σ. However, to fully compare the posteriors in the full range $-20 \leq A_0 \leq -5$, we need to extend the posteriors beyond the 5σ level, and a Gaussian extension is used to this end. This extension is detailed in Appendix B. In Appendix C we briefly review the Gaussian approximation that was used in R18.

4.5 X^2 statistics

We will now discuss how to quantify the compatibility between the posteriors $f(A_0|\text{galaxy}_g)$. In R18 we adopted the χ^2 statistic of equation (C2), whose $\chi^2_{\min}$ follows a χ^2 distribution with $k = N_g - 1$ degrees of freedom. Here, we improve upon the method of R18, performing a more accurate procedure that does consider the full posteriors $f(A_0|\text{galaxy}_g)$, instead of using Gaussian approximations based on the mean and the variance of $f(A_0|\text{galaxy}_g)$. Our new method is based on the Bayes factor (the ratio between two Bayesian evidences) and extends the χ^2 statistics to the general non-Gaussian case, reducing to it when the distributions $f(A_0|\text{galaxy}_g)$ are Gaussian. We name this generalization the X^2 statistics. It was inspired by the results of Verde et al. (2013); Lin & Ishak (2017).

First, following the notation of Verde et al. (2013); Lin & Ishak (2017), we introduce the Tension estimator $\mathcal{T}$, which is the Bayes factor defined as the ratio between a virtual hypothesis (Bayesian evidence $\bar{\mathcal{E}}$, see below) and the actual hypothesis (evidence $\mathcal{E}$):

$$\mathcal{T} = \frac{\bar{\mathcal{E}}}{\mathcal{E}}. \quad (26)$$

---

[3] See de Almeida et al. (2018) for a similar method, albeit for a different model.

We remind the reader that the Bayes factor gives the odds ratio relative to the two hypotheses and is a standard tool of Bayesian inference (see, e.g., Gregory 2010).

The evidence $\mathcal{E}$ is proportional to the integral of the product of the posteriors, that is,

$$\mathcal{E} = C \int dA_0 \prod_g f(A_0|\text{galaxy}_g), \quad (27)$$

where C is the constant of eq. (25). The value of C will not be relevant, as it will become clear shortly.

Similarly, the evidence $\bar{\mathcal{E}}$ is obtained according to

$$\bar{\mathcal{E}} = C \int dA_0 \prod_g \bar{f}(A_0|\text{galaxy}_g), \quad (28)$$

where $\bar{f}(A_0|\text{galaxy}_g)$ is the posterior of the g-th galaxy translated by the difference $A_0^{\text{gbv}} - A_{0g}^{\text{mean}}$ to a common reference point, the global best value A_0^{gbv}:

$$\bar{f}(A_0|\text{galaxy}_g) = f(A_0 + A_{0g}^{\text{mean}} - A_0^{\text{gbv}}|\text{galaxy}_g). \quad (29)$$

Note that C cancels out in equation (26). Eq. (29) implies that the mean A_{0g} according to the distribution $\bar{f}$ coincides with A_0^{gbv}. Therefore, the translated posteriors $\bar{f}(A_0|\text{galaxy}_g)$ overlap among themselves more than the original ones so that $\bar{\mathcal{E}} \geq \mathcal{E}$. The idea behind the Tension is to build an estimator that is sensitive to the degree of overlapping between different posteriors. In order to maximize the sensitivity of the Tension, one should translate the distributions in order to have $\mathcal{T} \geq 1$, that is, maximize the overlapping and so $\bar{\mathcal{E}}$. This is approximately achieved by translating the posteriors according to their distribution means A_{0g}^{mean} as in eq. (29). One could consider using the mode of A_{0g}, instead of the mean value; however, with the purpose of using Monte Carlo to simulate the expected distribution, it is preferable to use the mean value so that the MC data have a mean that reproduces the desired value. Nonetheless, we have verified that the difference between these choices is negligible, at least for this application.

The statistic X^2 is defined from the identification

$$X^2 \equiv 2\ln \mathcal{T} \geq 0, \quad (30)$$

which reduces to the χ^2 statistic of eq. (C2) if the distributions are Gaussian (Lin & Ishak 2017):

$$X^2 \longrightarrow \chi^2_{\min}, \quad (31)$$

so that X^2 follows a χ^2 distribution with $k = N_G - 1$ degrees of freedom. However, X^2 is well defined also in the general non-Gaussian case as one can compute the evidences without any approximation.

Now, in order to assess the significance of a value of X^2, we need the distribution of the X^2 statistic, which is expected to resemble the χ^2 distribution. In the general case it is not possible to obtain it analytically and one has to resort to a Monte Carlo simulation. The X^2 distribution is obtained under the null hypothesis that a fundamental A_0 exists. To this end we generate for each galaxy g a random value A_{0g}^{null} drawn from the numerical distribution $\bar{f}(A_0|\text{galaxy}_g)$: we use the full non-Gaussian distribution whose mean is at A_0^{gbv} in agreement with the null hypothesis. We then translate the distribution so that its mean is A_{0g}^{null}:

$$f_{\text{null}}(A_0|\text{galaxy}_g) = f(A_0 + A_{0g}^{\text{mean}} - A_{0g}^{\text{null}}|\text{galaxy}_g). \quad (32)$$
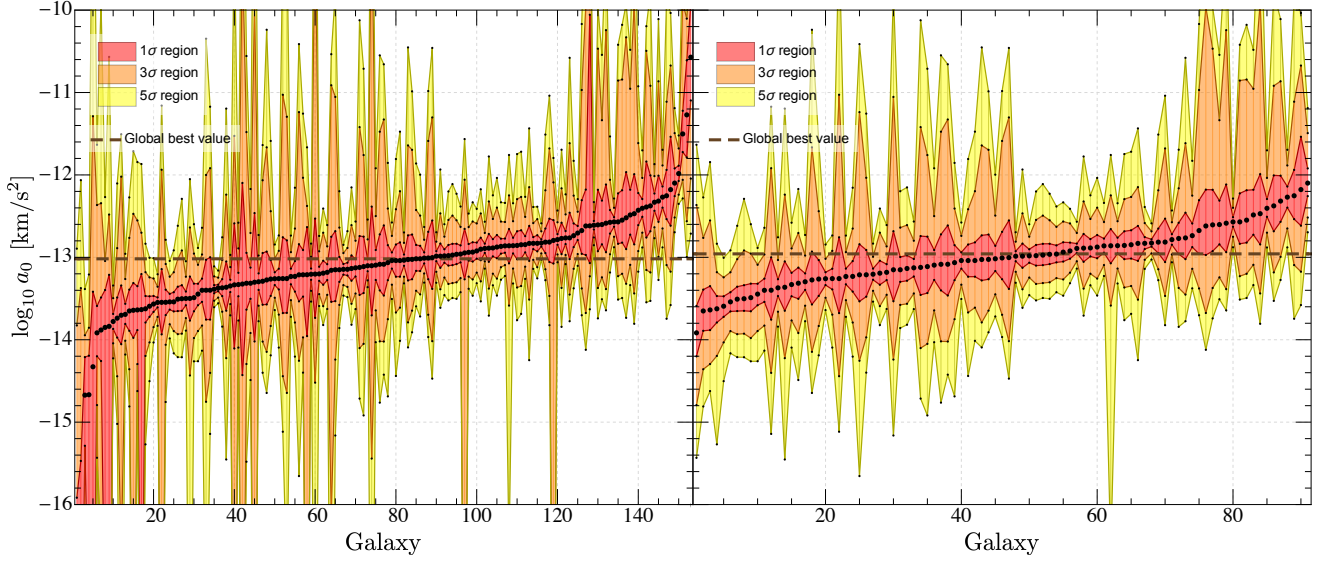
Figure 1. Posterior probability distributions of $A_0 \equiv \log_{10}[a_0/(\mathrm{km/s^2})]$ for each galaxy of the SPARC database that passed the quality cuts Q_1 (left, with 153 galaxies, the RAR sample $\mathcal{S}_1$) and $Q_1 \wedge Q_2$ (right, with 91 galaxies, the sample $\mathcal{S}_2$). Each posterior, for each galaxy, has been obtained after marginalizing over stellar mass-to-light ratios, galaxy distance and galaxy inclination, and are displayed showing the maximum (mode) of the posterior (large black dots) together with the 1, 3, and 5σ credible intervals (red, orange and yellow shaded regions, respectively). To enhance the clarity of the plot, the galaxies are sorted according to their posterior maximum, and small black dots are used to display the limits of the credible intervals for each galaxy. The global best value of A_0, for each of the cases, is shown with a dashed line: it is evident that many galaxies are not compatible with its value.

These posteriors can then be used to compute

$$\mathcal{E}^{\mathrm{null}} = C \int \mathrm{d}A_0 \prod_g f_{\mathrm{null}}(A_0|\mathrm{galaxy}_g) \,, \qquad (33)$$

$$X_{\mathrm{null}}^2 = 2 \ln \frac{\bar{\mathcal{E}}}{\mathcal{E}^{\mathrm{null}}} \,. \qquad (34)$$

By repeating many times the above algorithm one can generate numerically the X^2 distribution, from which one can compute the confidence in rejecting the null hypothesis. Although expensive, this method does not introduce any approximation and reduces to the well-known χ^2 distribution when the non-Gaussianity of the posteriors is small.

5 NUMERICAL METHODS

Our numerical procedure consists of the following pipeline divided into three stages:

(i) The first stage loads the SPARC data, sets the likelihood functions and priors for each galaxy (7), runs optimization procedures to find the best fit for each galaxy, exports the results. This stage is done with the MAGMA package.[4]

(ii) The second stage is the MCMC itself. After importing the last stage data, we use emcee,[5] an affine invariant sampler for Markov chain Monte Carlo (MCMC), to sample the posteriors $f(\theta|\mathrm{galaxy}_g)$. The best fits from the previous stage are used to set the starting conditions of the MCMC, reducing the needed computational time (we adopt a burn-in of 10%). Specifically, we computed chains of 50×10^6 total

points from 100 walkers, which is more than 100 times the autocorrelation time. The generated chains are exported. We have crosschecked that 45×10^6 points are enough in order to obtain reliable 5σ credible intervals (see Appendix A) by comparing the A_0 posteriors from emcee with those obtained via grid evaluation using mBayes,[6] which computes arbitrarily high credible intervals with negligible error.

(iii) The third stage analyzes the chains. We use getdist[7] for obtaining the credible intervals and the triangular plots (see, e.g., Figure A1). The analysis of the X^2 statistics is carried out using specialized numerical code for the two samples $\mathcal{S}_1$ and $\mathcal{S}_2$ discussed in Section 4.3. The X^2 distribution is obtained with a Monte Carlo (MC) simulation with 62×10^6 MC points for $\mathcal{S}_1$ and 123×10^6 MC points for $\mathcal{S}_2$.

6 RESULTS

We will now present our results for the two quality cuts discussed in Section 4.3. Figure 1 shows modes and 1, 3 and 5σ credible intervals of the posteriors $f(A_0|\mathrm{galaxy}_g)$ for the 153 galaxies that passed the quality cut Q_1 and the 91 galaxies that passed the combined $Q_1 \wedge Q_2$ quality cut: no single value of a_0 cuts through all the 5σ credible intervals. Also shown with a dashed line is the global best value of Section 4.4. From Figure 1 it is clear that many galaxies are not quite compatible with the global best value. The numerical values are given in Table 2.

Also in Table 2 we report the values of the X^2 statistic. For the sake of comparison we also report the values in

[4] github.com/davi-rodrigues/MAGMA (Rodrigues et al. 2018a)
[5] github.com/dfm/emcee (Foreman-Mackey et al. 2013)
[6] github.com/valerio-marra/mBayes (Camarena & Marra 2018)
[7] github.com/cmbant/getdist (Lewis 2019)

Table 1. Results for individual galaxies. The full table is provided as machine readable supplementary material. The columns are: (1) Galaxy name. (2) Best fit for $A_0 = \log_{10} a_0$ [km/s^2]. (3) Minimum χ^2 value. (4) Number of rotation curve data points. (5) Part a of the quality cut Q_2. (6) Part b of the quality cut Q_2. A '1' is used if the galaxy passes a quality cut and 0 is used otherwise. In order to pass the Q_2 quality cut, both Q_{2a} and Q_{2b} need to be 1. (7) The mode of the marginalized A_0 posterior. (8-13) The limits of the A_0 credible intervals, with respect to the A_0 mode, for 1σ, 3σ and 5σ.

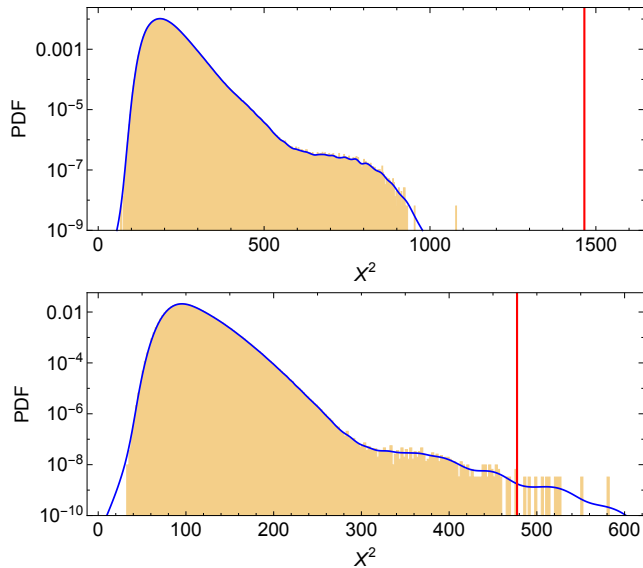| Galaxy (1)	A_0 best fit (2)	$\chi^2_{\min}$ (3)	N (4)	Q_{2a} (5)	Q_{2b} (6)	A_0 mode (7)	$1\sigma_-$ (8)	$1\sigma_+$ (9)	$3\sigma_-$ (10)	$3\sigma_+$ (11)	$5\sigma_-$ (12)	$5\sigma_+$ (13)
CamB	-14.645	38.884	9	1	0	-14.672	-0.614	0.462	-5.328	0.727	-5.328	1.287
D512-2	-13.241	0.297	4	1	0	-13.258	-0.416	0.463	-1.388	1.963	-3.752	4.179
D564-8	-13.486	8.546	6	1	1	-13.502	-0.147	0.164	-0.424	0.585	-0.710	1.212
D631-7	-13.140	183.494	16	0	1	-13.145	-0.075	0.080	-0.214	0.259	-0.337	0.462
DDO064	-13.030	3.712	14	1	1	-13.085	-0.317	0.363	-0.935	1.609	-1.679	2.535
...	...	...	...	...	...	...	...	...	...	...	...	...

Figure 2. Numerical distribution of the X^2 statistic that generalizes the χ^2 statistic to the case of non-Gaussian distributions. The filled yellow histogram was obtained numerically using a Monte Carlo simulation. The blue solid line is the smoothed empirical distribution. The vertical red line marks the values X^2 reported in Table 2. The hypothesis that there is a fundamental acceleration scale is ruled out with the confidence of $> 5.7\sigma$ for $\mathcal{S}_1$ and of 5.3σ for $\mathcal{S}_2$.

Table 2. Numerical results for the two samples $\mathcal{S}_1$ and $\mathcal{S}_2$. Top: results with the tension-based method as here proposed. Bottom: for comparison's sake we report also the results that adopt the Gaussian approximation, following the R18 methodology. The hypothesis that there is a fundamental acceleration scale is ruled out with a confidence larger than 5σ.

Tension-based method	$\mathcal{S}_1$ (RAR sample)	$\mathcal{S}_2$
a_0^{gbv} [km/s^2]	0.96×10^{-13}	1.10×10^{-13}
X^2	1465	477
rejection of fundamental a_0	$> 5.7\sigma$	5.3σ
R18 Gaussian method	$\mathcal{S}_1$ (RAR sample)	$\mathcal{S}_2$
a_0^{gbv} [km/s^2]	0.91×10^{-13}	1.06×10^{-13}
$\chi^2_{\min}$	1280	438
rejection of fundamental a_0	28σ	14σ

the Gaussian approximation, under which $X^2 \to \chi^2_{\min}$. Under this approximation one can compute the confidence of rejecting the hypothesis that there is a fundamental acceleration scale using the χ^2 distribution. For the sample $\mathcal{S}_2$ one finds 14σ. If we approximate the χ^2 distribution itself as a Gaussian, as done in R18, the confidence is 26σ. This is due to the fact that the tail of the χ^2 distribution is longer than the one of the corresponding Gaussian.

About the results above using the Gaussian approximation, we comment that this latter value (26σ) is in qualitative agreement with the results of Chang & Zhou (2019). They considered the quality cut Q_2, but not in the same way we are doing here. They eliminated the same galaxies that were eliminated in R18 due to that quality cut Q_2 in that

reference (leaving a sample size of 100 galaxies). However, R18 uses different priors, and the Q_2 quality cut depends on the priors. Here we reselect the galaxies to be removed considering the quality cuts, thus the resulting sample of galaxies, when Q_2 is applied, is different with respect to R18 and Chang & Zhou (2019). This difference on the sample of galaxies naturally leads to a difference on the face-value confidence in rejecting the fundamental acceleration scale (although, we stress, there is no conflict on the conclusions). At last, we also recall that the priors used by Chang & Zhou (2019) are very similar to the priors of Li et al. (2018) and the ones that we use here, but they are not identical, which may be the reason of some differences on the length of the 5σ credible intervals.[8]

Here we go beyond the Gaussian approximation of R18 and therefore we adopt the non-Gaussian X^2 value. In order to assess its significance, we compute the X^2 distribution according to the null hypothesis that a fundamental accel-

---

[8] The 5σ credible intervals that we find here are on average slightly larger than those of Chang & Zhou (2019). Besides the use of slightly different priors, the discrepancy could be due to the fact that one needs a large number of MCMC points in order to reliably sample 5σ credible intervals.

eration scale exists. We adopt the Monte Carlo simulation described in Sections 4.5 and 5. The result is given in Figure 2: the observed X^2 values are shown with a red line. It is evident that they lie deep into the tail of the distribution, which is modeled in a robust way. Finally, we estimate the PDF by smoothing the empirical distribution (in light orange) via an adaptive Gaussian kernel. The result is shown with a blue line in Figure 2.

Regarding $\mathcal{S}_1$, none of the MC points fall near the observed value. As we generated 62×10^6 points and none was greater than the observed one, we can conclude, very conservatively, that the null hypothesis is ruled out at $> 5.7\sigma$. Regarding $\mathcal{S}_2$, out of the total 123×10^6 MC points, we obtained 11 MC values greater than the observed one so that we can conclude that the null hypothesis is ruled out with the high confidence of 5.3σ. Using the smoothed distribution (blue curve in Figure 2) we obtain the same significance. The significance is lower as compared to the Gaussian case because the non-Gaussian distributions of individual galaxies features, on average, longer tails (Rodrigues et al. 2020; Cameron et al. 2020).

7 CONCLUSIONS

This work stresses further the importante of testing the compatibility between the acceleration scales derived from the individual galaxies, denoted by $A_{0g} = \log_{10} a_{0g}$ [km/s], where g is an index that labels the galaxies. Such test is important for understanding the meaning of MOND and the RAR, and it is a fundamental test for MOND, since it tests one of the cornerstone assumptions of MOND (the universality of a_0) in the context that most favors MOND, that of rotationally supported galaxies. This work improves the methodology of R18, confirming its results that, in the context of rotationally supported galaxies, the Radial Acceleration Relation (RAR) is an emergent correlation. To achieve this conclusion, in summary, we assume that the function that expresses the RAR correlation (the interpolating function) is common to all the galaxies, but the value of the RAR acceleration scale $a_†$ is not used. For the acceleration scale we use a free constant a_{0g} for each galaxy. Then we test, using Bayesian inference, whether the individual a_{0g} constraints found for each one of the galaxies are compatible among themselves (this requires the computation of the marginalized posteriors on a_{0g}, and this cannot be found from best fits alone). With the improved methods presented here, we find that the RAR does not imply a fundamental property of (rotationally supported) galaxies but rather an emergent behavior. In this way, we have confirmed that there is a strong evidence against a common a_0 value: a fundamental acceleration scale a_0 is rejected at more than 5σ.

This behaviour is not in contradiction with standard dark matter interpretations, but it is at odds with MOND, if the latter is assumed to be a fundamental law at the level of (rotationally supported) galaxies. If MOND is viewed as an empirical approximation relation, then MOND is essentially the RAR: a phenomenological and simple rule valid for galaxies that captures certain average dynamics whose underlying physics is more complex. From this perspective, it is a useful correlation that, at the moment, it has no clear contradiction with the standard dark matter picture (Stone

& Courteau 2019), but see Ren et al. (2019) for possible hints on an underlying non-standard dark matter physics. Also, some of the RAR features can be seen as necessary consequences of galaxy evolution in a dark matter context (Ludlow et al. 2017; Navarro et al. 2017; Dutton et al. 2019).

On the new methodology used here, besides using essentially the same priors of Li et al. (2018), we go beyond the Gaussian approximation that R18 adopted in order to quantify the tension between the posteriors on a_0. Here we have introduced the X^2 statistics, based on the Tension estimator $\mathcal{T}$ proposed by Verde et al. (2013), which in turn is based on the Bayes factor (e.g., Gregory 2010; Jeffreys 2011). The X^2 statistics extends the χ^2 statistics to the general non-Gaussian case, reducing to it when the variables follow a Gaussian distribution. We expect the X^2 statistics to have useful applications in other contexts.

In order to rule out the possibility that our results are driven by outliers, we have carried out the analysis using two different quality cuts. The first is the same quality cut used to evaluate the RAR (leading to what we call the RAR sample). Using this quality cut we found that the hypothesis that there is a fundamental acceleration scale is ruled out with the a confidence clearly larger than 5.7σ. Then we considered a stronger quality cut based on statistical arguments that could indicate a lower chance of determining an accurate A_0 value. This is a strong quality cut that reduced the sample size by $\sim 60\%$, with many cases of very low and very high A_0 values being removed. But even with this quality cut a fundamental acceleration scale is ruled out with a confidence larger than 5σ. Therefore, our results are robust also regarding outliers.

REFERENCES

Andrae R., Schulze-Hartung T., Melchior P., 2010, [1012.3754].
Camarena D., Marra V., 2018, Phys. Rev., D98, 023537, [1805.09900].
Cameron E., Angus G. W., Burgess J. M., 2020, Nat. Astron., p. 15.
Chang Z., Zhou Y., 2019, MNRAS, 486, 1658, [1812.05002].
Dutton A. A., Macciò A. V., Obreja A., Buck T., 2019, MNRAS, 485, 1886, [1902.06751].
Famaey B., McGaugh S., 2012, Living Rev. Rel., 15, 10, [1112.3960].
Fattahi A., Navarro J. F., Frenk C. S., Oman K. A., Sawala T., Schaller M., 2018, MNRAS, 476, 3816, [1707.03898].
Foreman-Mackey D., Hogg D. W., Lang D., Goodman J., 2013, Publ. Astron. Soc. Pac., 125, 306, [1202.3665].

Frandsen M. T., Petersen J., 2018, [1805.10706].

Gentile G., Famaey B., de Blok W., 2011, A&A, 527, A76, [1011.4148].

Gregory P. C., 2010, Bayesian logical data analysis for the physical sciences : a comparative approach with Mathematica support. Cambridge University Press, Cambridge New York.

Jeffreys H., 2011, Scientific Inference. Muller Press.

Kent S. M., 1987, Astron. J., 93, 816.

Kroupa P., et al., 2018, Nat. Astron., 2, 925, [1811.11754].

Lelli F., McGaugh S. S., Schombert J. M., 2016, AJ, 152, 157, [1606.09251].

Lewis A., 2019, [1910.13970].

Li P., Lelli F., McGaugh S., Schormbert J., 2018, Astron. Astrophys., 615, A3, [1803.00022].

Lin W., Ishak M., 2017, Phys. Rev., D96, 023532, [1705.05303].

Ludlow A. D., et al., 2017, Phys. Rev. Lett., 118, 161103, [1610.07663].

McGaugh S. S., 2004, Astrophys. J., 609, 652, [astro-ph/0403610].

McGaugh S., Lelli F., Schombert J., 2016, Phys. Rev. Lett., 117, 201101, [1609.05917].

McGaugh S. S., Li P., Lelli F., Schombert J. M., 2018, Nat. Astron..

Meidt S. E., et al., 2014, ApJ, 788, 144, [1402.5210].

Milgrom M., 1983, ApJ, 270, 371.

Milgrom M., 1988, ApJ, 333, 689.

Milgrom M., 2015, Phys. Rev., D92, 044014, [1507.05741].

Milgrom M., 2016, [1609.06642].

Mo H., van den Bosch F., White S., 2010, Galaxy Formation and Evolution. Cambridge University Press.

Navarro J. F., Benítez-Llambay A., Fattahi A., Frenk C. S., Ludlow A. D., Oman K. A., Schaller M., Theuns T., 2017, MNRAS, 471, 1841, [1612.06329].

Profumo S., 2017, Introduction To Particle Dark Matter, An (Advanced Textbooks in Physics). WSPC (EUROPE).

Querejeta M., et al 2015, ApJS, 219, 5, [1410.0009].

Randriamampandry T., Carignan C., 2014, MNRAS, 439, 2132, [1401.5619].

Ren T., Kwa A., Kaplinghat M., Yu H.-B., 2019, Phys. Rev., X9, 031020, [1808.05695].

Rodrigues D. C., Marra V., Del Popolo A., Davari Z., 2018a, Nat. Astron., 2, 668, [1806.06803].

Rodrigues D. C., Marra V., Del Popolo A., Davari Z., 2018b, Nat. Astron., 2, 927, [1811.05882].

Rodrigues D. C., Marra V., Del Popolo A., Davari Z., 2020, Nat. Astron., 4, 134, [2002.01970].

Sanders R. H., 1990, A&ARv, 2, 1.

Stone C., Courteau S., 2019, ApJ, 882, 6, [1908.06105].

Verde L., Protopapas P., Jimenez R., 2013, Phys. Dark Univ., 2, 166, [1306.6766].

Zhou Y., Del Popolo A., Chang Z., 2020, Phys. Dark Univ., 28, 100468.

de Almeida Á. O. F., Amendola L., Niro V., 2018, JCAP, 1808, 012, [1805.11067].

de Blok W. J. G., McGaugh S. S., 1998, ApJ, 508, 132, [astro-ph/9805120].

APPENDIX A: 5σ CREDIBLE INTERVALS

As an example, in Figure A1 we show the triangular plot that illustrates the MCMC exploration of the posterior $f(\theta|\text{UGC } 03205)$. As another example, in Figure A2 we show the marginalized MCMC histogram (orange shade) and the corresponding smoothed marginalized posterior $f(A_0|\text{F574-1})$ (black line). The fact that the MCMC points span the 5σ interval shows that the adopted number of 45×10^6 points is adequate.

APPENDIX B: POSTERIOR DISTRIBUTION EXTENSION BEYOND 5σ

In order to proceed as described in Sections 4 one needs to have posterior distributions $f(A_0|\text{galaxy}_g)$ defined in the common prior interval $-20 \leq A_0 \leq -5$. We obtained the posteriors using a very large number of MCMC points (45×10^6), which is enough to reliably obtain 5σ credible intervals. These posteriors, however, do not span the interval $-20 \leq A_0 \leq -5$ as it is not numerically viable to reconstruct the posteriors up to, e.g., $> 10\sigma$. In order to overcome this technical difficulty, we extended the distributions $f(A_0|\text{galaxy}_g)$ beyond their 5σ intervals using the following Gaussian tails as defined in eq. (B1). In that equation, $const \simeq 1$ is a normalization constant, $A_0^{\min} \leq A_0 \leq A_0^{\max}$ is the region covered by the MCMC chain, and A_{0g}^{mean} and σ_g are mean and standard deviation relative to $f(A_0|\text{galaxy}_g)$.

APPENDIX C: REVIEW ON THE GAUSSIAN APPROXIMATION METHOD

For completeness, and since it will be useful for comparing with our newer results, we briefly review below the Gaussian approximation and χ^2 statistics that we used in R18.

In R18 we computed the global best value by approximating the posteriors $f(A_0|\text{galaxy}_g)$ as Gaussians, that is, we neglected higher moments,

$$f(A_0|\text{galaxy}_g) \approx f_{\text{gau}}(A_0|\text{galaxy}_g) \equiv \mathcal{N}(A_{0g}^{\text{mean}}, \sigma_g), \quad \text{(C1)}$$

where A_{0g}^{mean} and σ_g are mean and standard deviation relative to $f(A_0|\text{galaxy}_g)$. Maximizing $\prod_g f_{\text{gau}}(A_0|\text{galaxy}_g)$ is equivalent to minimizing the following χ^2 function (as done in R18):

$$\chi^2(A_0) = \sum_{g=1}^{N_G} \frac{(A_{0g}^{\text{mean}} - A_0)^2}{\sigma_g^2}, \quad \text{(C2)}$$

so that $\chi^2(A_0^{\text{gbv}}) = \chi^2_{\min}$.

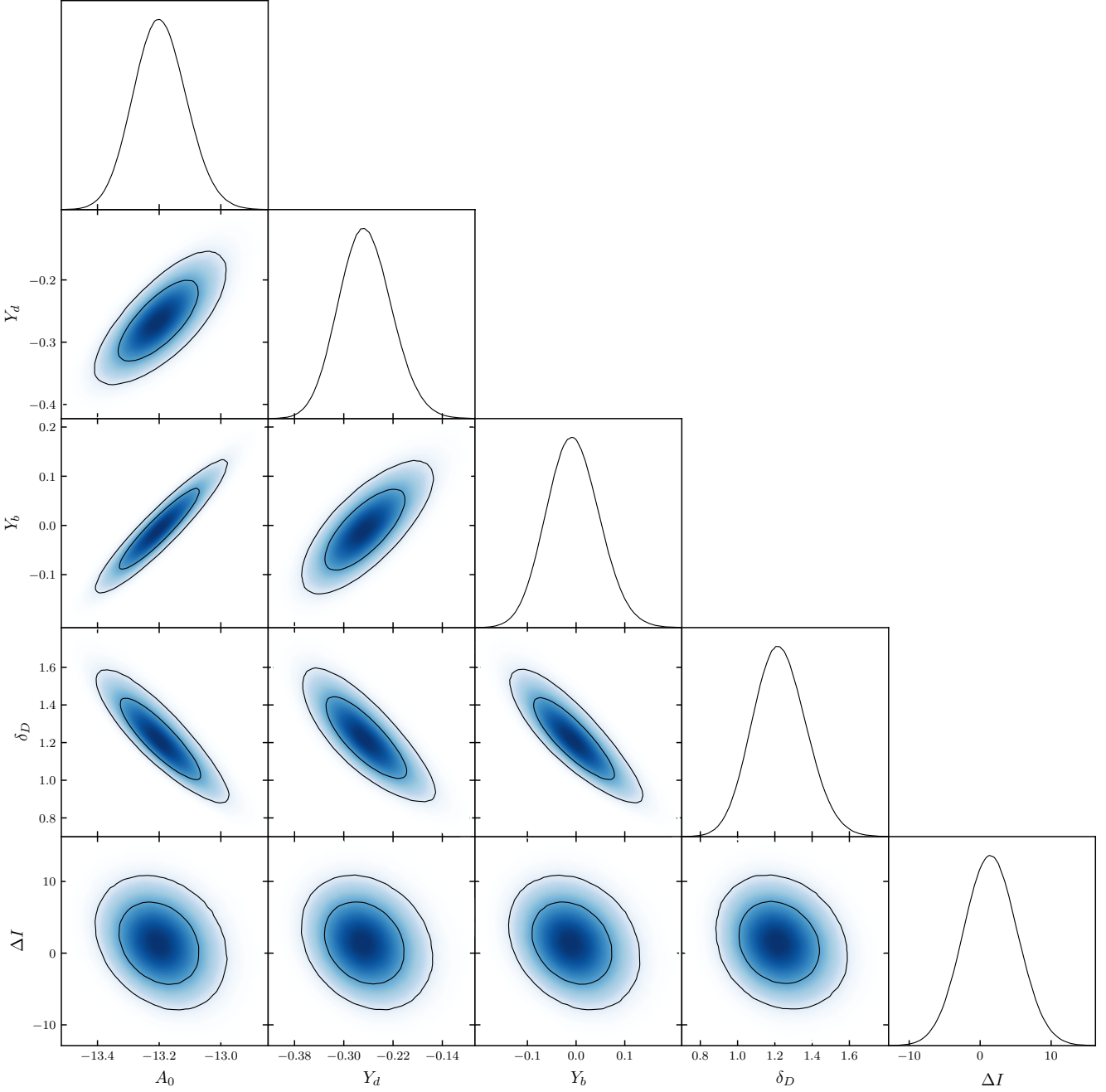This paper has been typeset from a TeX/LaTeX file prepared by the author.

Figure A1. Marginalized 1 and 2σ contours for the galaxy UGC 03205 of the SPARC dataset. Here, $\delta_D = D/D_0$ and $\Delta I = I - I_0$.

$$f^{\text{ext}}(A_0|\text{galaxy}_g) = const \times \begin{cases} f(A_0^{\min}|\text{galaxy}_g) \exp\left[\frac{(A_0^{\min} - A_{0g}^{\text{mean}})^2 - (A_0 - A_{0g}^{\text{mean}})^2}{2\sigma_g^2}\right] & -20 \leq A_0 \leq A_0^{\min} \\ f(A_0|\text{galaxy}_g) & A_0^{\min} \leq A_0 \leq A_0^{\max} \\ f(A_0^{\max}|\text{galaxy}_g) \exp\left[\frac{(A_0^{\max} - A_{0g}^{\text{mean}})^2 - (A_0 - A_{0g}^{\text{mean}})^2}{2\sigma_g^2}\right] & A_0^{\max} \leq A_0 \leq -5 \end{cases} \quad \text{(B1)}$$
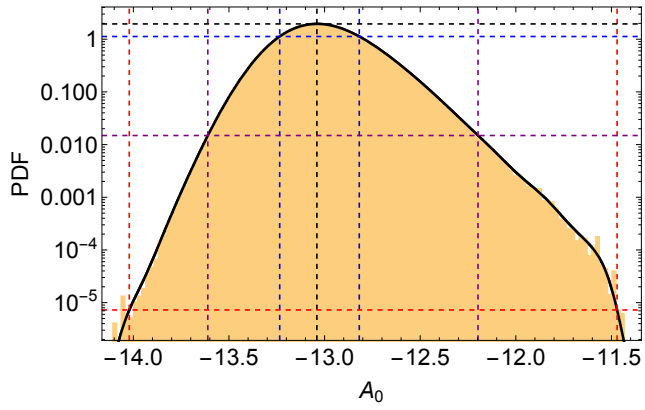
Figure A2. Marginalized MCMC histogram (orange shade) and corresponding smoothed marginalized posterior $f(A_0|\text{F574-1})$ (black line). The dashed black horizontal and vertical lines mark the mode. The blue, purple and red lines mark the 1, 3 and 5σ credible intervals, respectively.